

## ARTICLE

Electrochemical CO<sub>2</sub> Reduction on Pd-Modified Cu Foil

Zhi-juan Sun, Matthew M. Sartin<sup>†</sup>, Wei Chen, Fan He, Jun Cai, Xu-xu Ye, Jun-ling Lu, Yan-xia Chen\*

Hefei National Laboratory for Physical Sciences at the Microscale and Department of Chemical Physics, University of Science and Technology of China, Hefei 230026, China

(Dated: Received on April 25, 2019; Accepted on May 31, 2019)

Bimetallic catalysts can improve CO<sub>2</sub> reduction efficiency via the combined properties of two metals. CuPd shows enhanced CO<sub>2</sub> reduction activity compared to copper alone. Using differential electrochemical mass spectrometry (DEMS) and electrochemical infrared (IR) spectroscopy, volatile products and adsorbed intermediates were measured during CO<sub>2</sub> and CO reduction on Cu and CuPd. The IR band corresponding to adsorbed CO appears 300 mV more positive on CuPd than that on Cu, indicating acceleration of CO<sub>2</sub> reduction to CO. Electrochemical IR spectroscopy measurements in CO-saturated solutions reveal similar potentials for CO adsorption and CO<sub>3</sub><sup>2-</sup> desorption on CuPd and Cu, indicating that CO adsorption is controlled by desorption of CO<sub>3</sub><sup>2-</sup>. DEMS measurements carried out during CO reduction at both electrodes showed that the onset potential for reduction of CO to CH<sub>4</sub> and CH<sub>3</sub>OH on CuPd is about 200 mV more positive than that on Cu. We attribute these improvements to interaction of Cu and Pd, which shifts the d-band center of the Cu sites.

**Key words:** CO<sub>2</sub> reduction, CH band, CuPd activity, Differential electrochemical mass spectrometry, Attenuated total reflection Fourier transform infrared spectroscopy

## I. INTRODUCTION

The activity and selectivity of CO<sub>2</sub> electroreduction on metals partly depends on the strength of CO adsorption [1, 2]. CO<sub>2</sub> reduction occurs through similar initial steps on all metals, but different adsorption energies for the intermediates on each kind of metal dictate the path the reaction will take [3]. Among the metals explored, copper is one of the most widely studied. Because the adsorption of CO on Cu is neither too weak to catalyze CO reduction, nor strong enough to poison the catalyst [2, 4, 5], copper is the most effective metal for the reduction of CO<sub>2</sub>/CO to hydrocarbons instead of HCOOH [6, 7]. However, the onset potential of CO reduction on copper is always high [8]. Usually on a pure copper electrode, the onset potential for reduction is about -1.1 V *vs.* SHE [9], which is similar to that of hydrogen evolution on copper, resulting in competition between the two processes [4, 10, 11]. For the formation of CH<sub>4</sub> and C<sub>2</sub>H<sub>4</sub>, the potential can be even

more negative [12]. It is therefore necessary to lower the onset potential. In order to improve the yields and onset potentials of complex hydrocarbons generated from CO<sub>2</sub> reduction, it is important to consider the interactions that different metals have with all of the intermediates of the process, rather than just adsorbed CO or CO<sub>2</sub> [13]. Compared with copper, Pt group metals have lower overpotentials for the reduction of CO<sub>2</sub> to CO or HCOOH [14]. There have been several attempts to modify the catalyst surface, in order to improve the activity and product selectivity of CO<sub>2</sub> reduction. A few examples have been reported including roughening the surface [15–17], plasma activation [18], and introduction of Pt group metals on copper.

Takashima *et al.* [19] demonstrated increased Faradaic efficiency for formate production (84%) on copper-modified Pd nanoparticles. This is 15% more than that observed on Pd nanoparticles. Li *et al.* [20] used a Pd<sub>7</sub>Cu<sub>3</sub> electrode and observed a Faradaic efficiency for CO production of 80%. They attribute this enhancement to the greater number of active sites on the bimetallic catalyst. Pd binds to CO<sub>2</sub> and COOH\* more strongly than copper, while copper promotes the desorption of the intermediate, CO. The combination of metals thus favors more products and suppresses competing reactions. Zhang *et al.* [14] deposited layers of different thickness of copper on Pd (octahedron tetrahedron), Pd(111), and Pd(310). For a 1 monolayer (ML) coating, it was found that the ethanol production efficiency could be affected by the shape of the Pd

<sup>†</sup>Current address: State Key Laboratory of Physical Chemistry of Solid Surfaces, Collaborative Innovation Center of Chemistry for Energy Materials (iChEM), MOE Key Laboratory of Spectrochemical Analysis & Instrumentation, College of Chemistry and Chemical Engineering, Xiamen University, Xiamen 361005, China

\*Author to whom correspondence should be addressed. E-mail: yachen@ustc.edu.cn, Tel.: +86-551-63600035

core. The Faradaic current for ethanol production with  $\text{Cu}_{1\text{ML}}/(\text{octahedron tetrahedron})\text{-Pd}$  nanocubes (NCs) is 20.4%. This is considerably higher than that on  $\text{Cu}_{1\text{ML}}/(\text{111})\text{-faceted Pd}$  NCs, which show only 6.1% efficiency for ethanol production. DFT calculations have shown that Pd coated with 1 ML of Cu exhibits moderate CO adsorption. However, variations between the data presented by different groups show the need for an understanding of this reaction under simpler conditions.

Previous studies have focused on the selectivity for various products obtained when performing  $\text{CO}/\text{CO}_2$  reduction using different metals with different crystal facets. There are also many studies in which copper was deposited on a Pt group metal, such as Au [21], Pt [22], and Pd [14, 19]. The advantage of using a bimetallic catalyst is that there is a synergetic effect between the two metals that can yield overall improvement in the catalytic properties of the individual components. Among metals to pair with Cu, Pd is one of the most popular choices [14, 19, 20]. Neighboring Pd atoms can change the electronic structure of Cu, and improve its reducing capability. Theory has shown that as the coordination number of Cu decreases, the d-band center shifts towards the Fermi energy, leading to stronger adsorption of H to the surface and lower  $\Delta G_{\text{H}}$  [23]. The enhanced H adsorption can provide a source of H for the further production of hydrocarbons. The binding energy for CO on Pd is higher than on Cu, giving rise to a greater surface coverage of CO and H, which facilitates generation of  $\text{CH}_4$  [24]. Here, we have used atomic layer deposition (ALD) to deposit Pd on Cu, in order to examine how the bimetallic catalyst affects  $\text{CO}_2$  reduction adsorbates, product generation onset potentials, and product selectivity. By using differential electrochemical mass spectrometry (DEMS) to measure the generation of volatile products *in situ*, we observe low overpotentials for the reduction of CO to  $\text{CH}_4$  and  $\text{CH}_3\text{OH}$ . In addition, we combined the electrochemical experiment with Fourier transform infrared (FTIR) spectroscopy in an attenuated total reflection configuration (electrochemical ATR-FTIR spectroscopy) to monitor the adsorbates generated during the reaction and to correlate the amount of adsorbed CO with the product generation.

## II. EXPERIMENTS

### A. Materials and characterization

$\text{NaHCO}_3$  (99.998%, Puratronic) and  $\text{CuSO}_4 \cdot 5\text{H}_2\text{O}$  (99.999%, Puratronic) were purchased from Alfa Aesar. CO (99.99%), Ar (99.999%), and  $\text{N}_2$  (99.999%) were purchased from Linde. All other chemicals were purchased from Sinopharm Chemical Reagent Co. Ltd. CO- and  $\text{CO}_2$ -saturated solutions were prepared by bubbling the electrolyte solution with the corresponding gas for at least 20 min. The resulting pH values

were 8.3 and 6.8, respectively.

### B. Electrode preparation and ATR-FTIR measurements

ATR-FTIR measurements were carried out in a 3-electrode configuration. A CHI 700 (CH Instruments, Shanghai, China) was used to control the working electrode potential. The counter and reference electrodes were an Au wire and Ag/AgCl, respectively. The gold wire was chosen as the counter electrode due to the problem of metal ions which were generated by oxidation of the counter electrode and deposited on the working electrode during  $\text{CO}/\text{CO}_2$  reduction [25]. Although the amount of metal deposited in this way is very small, signals corresponding to CO adsorbed on these metal deposits can be detected by ATR-FTIR and can lead to misinterpretation of the data, as has been previously shown in experiments performed using a Pt counter electrode [25, 26]. The effect is minimized by using Au, because CO only weakly adsorbs to gold, and it is fully desorbed from Au at  $-0.5\text{ V vs. SHE}$ , which is near the onset potential for CO adsorption on Cu [25]. In our experiment, at  $-0.2\text{ V vs. SHE}$ , the potential of the highest coverage of CO adsorbed onto gold [25, 27], there is no detectable IR absorption band corresponding to CO adsorbed to gold. This demonstrates that if there is any gold on the surface, it is such a small amount that it does not impact the results of the ATR-FTIR experiments. Therefore, results discussed here can be interpreted in terms of the effects of CO on copper and palladium. All potentials were converted to standard hydrogen electrode (SHE). The working electrode was prepared by plating a copper film onto the silicon prism.

The preparation of the copper film is as follows. The reflecting plane of the silicon was polished using diamond paste, with progressively smaller particle sizes, down to  $0.25\ \mu\text{m}$ . The polished prisms were boiled in a solution of  $\text{NH}_4\text{OH}:\text{H}_2\text{O}_2:\text{H}_2\text{O}=1:1:5$  by volume for 10 min, followed by a solution of  $\text{HCl}:\text{H}_2\text{O}_2:\text{H}_2\text{O}=1:1:5$  by volume for 10 min. The surfaces were then thoroughly washed and immersed in a  $17.8\ \text{mol/L NH}_4\text{F}$  solution for about 1 min to make the surface hydrophobic. Cu seeds were grown by immersing the hydrophobic surface into a solution of  $0.625\ \text{mol/L HF}$  and  $3.15\ \text{mol/L CuSO}_4 \cdot 5\text{H}_2\text{O}$  for 10–20 s. After washing with deionized water, the prism was placed in a water bath set to  $30\ ^\circ\text{C}$ , with the surface exposed to the air. About 1 mL plating solution was added onto the prism to grow the copper film for 5–6 min [28]. The resistance measured between two corners of the prism was typically  $8\ \Omega$ .

Pd atomic layer deposition (ALD) was carried out in a viscous flow reactor (GEMSTAR-6TM Benchtop ALD, Arradiance) at  $120\ ^\circ\text{C}$  using palladium hexafluoroacetate ( $\text{Pd}(\text{hfac})_2$ , Sigma-Aldrich, 99.9%) and formalin (Aldrich, 37% HCHO and 15%  $\text{CH}_3\text{OH}$  in aqueous solution). Ultrahigh purity  $\text{N}_2$  (99.999%) was

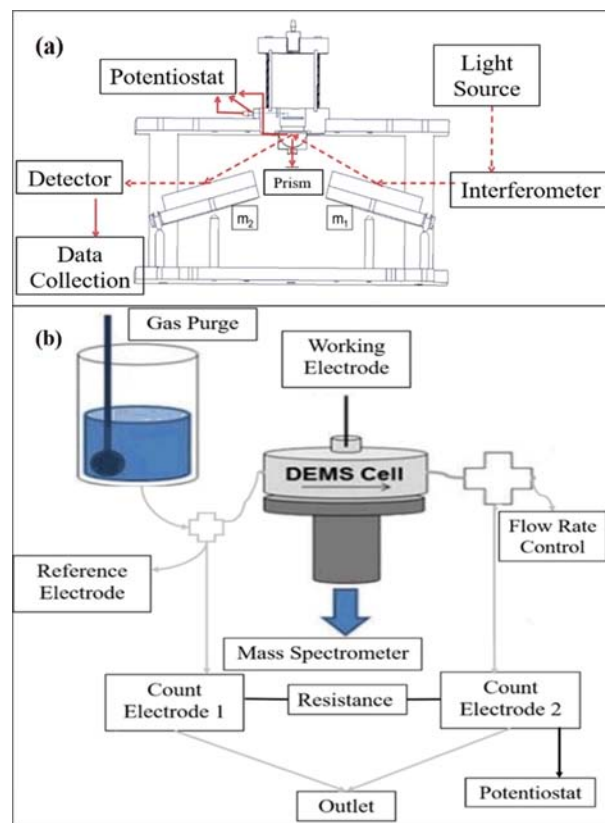
used as a carrier gas at a flow rate of 200 mL/min. The Pd(hfac)<sub>2</sub> precursor container was heated to 65 °C to reach sufficient vapor pressure. The chamber was heated to 120 °C, and the inlet manifold was maintained at 115 °C to avoid precursor condensation. The time for Pd(hfac)<sub>2</sub> exposure, N<sub>2</sub> purge, formalin exposure, and N<sub>2</sub> purge was 40, 120, 60, and 120 s, respectively. The presence of Pd on the prism was verified in separate experiments by dissolving the film in aqua regia and using an Inductively-Coupled Plasma Atomic Emission Spectrometer (ICP-AES, Optima 7300 DV, Perkin-Elmer), with detection limit of 0.01 µg/mL for Cu and Pd. The concentrations of Pd and Cu were found to be 0.765 and 4.328 µg/mL, respectively.

The film-coated prism was then fixed in a home-made cell, and the cell was filled with about 15 mL electrolyte solution. IR spectra were recorded using a commercially-available FTIR spectrometer (FTS-7000E, Varian, Palo Alto, CA) with a liquid N<sub>2</sub>-cooled MCT detector. All spectra were constructed from an average of 16 scans recorded at 20 kHz, with 4 cm<sup>-1</sup> spectral resolution, giving a time-resolution of 5 s (25 mV) per spectrum. The spectrum accumulated for 60 scans at the initial potential of the experiment was used as the reference spectrum. All absorption spectra are presented in unit of mOD, defined as  $-1000 \log(R/R_0)$ , where  $R$  and  $R_0$  are the reflected IR light intensities recorded at the measured and reference potentials, respectively. A schematic of the IR spectrometer is provided in Scheme 1(a).

### C. DEMS measurements

DEMS measurements were performed using a 3-electrode configuration in a dual-thin-layer flow-cell (flow rate=10 µL/s). The Ag/AgCl reference electrode and one of two Pt wire counter electrodes were placed upstream from the working electrode, separated from the flow path by long tubes to prevent contamination caused by leakage from the reference electrode or products generated at the counter electrode. A second counter electrode was placed downstream from the working electrode and connected to the first counter electrode by a 20 MΩ resistor. The potentiostat was directly connected to the second counter electrode. Note that, with this configuration, it is not necessary to use a gold counter electrode, as any Pt generated by oxidation of the counter electrode will flow out of the cell without interacting with the working electrode. The products generated at the working electrode were analyzed using a Hiden HPR-40 DSA Bench Top-Membrane Inlet Gas Analysis System. A schematic of the solution flow path for the DEMS setup is presented in Scheme 1(b).

The working electrode used for the experiments was a commercially available copper foil, cut to a disk shape and attached to a glassy-carbon electrode (6 mm in diameter) using a conductive carbon adhesive. Prior



Scheme 1 (a) Schematic of the cell-holder and light path for *in-situ* electrochemical ATR-FTIR spectroscopy measurements. (b) Schematic for solution flow path used for DEMS experiments. Arrows represent the path of solution flow, and black lines represent wires connecting the various parts of the electrochemical cell.

to each experiment, the foil was rinsed with concentrated phosphoric acid for 10 min, to remove copper oxide, sonicated in absolute ethanol and water to remove impurities, and then dried with nitrogen. Electropolishing was then performed in an electrochemical cell for 180 s at +2.0 V. For the experiments in which the working electrode was CuPd, the same cleaning procedure was performed on the copper foil, and Pd was then deposited on the Cu foil using ALD, as described for the IR experiments.

## III. RESULTS AND DISCUSSION

### A. Dependence of CO<sub>2</sub> reduction intermediates on ambient temperature

Before comparing the results obtained on Cu with those obtained on CuPd, it is necessary to discuss how variation in ambient temperature may affect the results. The temperature in our laboratory is not well-controlled, so the experimental temperature varies throughout the year, and it is generally  $\pm 4$  °C of the

outside temperature, being slightly cooler in summer and slightly warmer in winter. Comparison of data between CuPd and Cu was performed in winter, when the average temperature is fairly low. Researchers comparing their results to ours should keep this in mind. Therefore, we first discuss how variations in the outside temperature can affect the results. There are two primary ways which can occur: electrode structural changes caused by changes in the deposition time and changes in the reaction pathway, caused by the differences in reaction temperature. To make this comparison, we examined the *in-situ* electrochemical ATR-FTIR spectra obtained at two different time during a year. For prisms prepared in June, when the temperature in Hefei, Anhui, China, where our laboratory is located, can approach 34 °C, and the indoor laboratory temperature was about 30 °C, copper seeds were grown for 10–15 s, and deposition time was 4.5 min. We refer to the electrode prepared in this condition as Cu-Jun. On the other hand, in February, when the outside temperature was typically near 0 °C, resulting in a laboratory temperature near 4 °C, the copper seeds were grown for 20 s, and the deposition was carried out for 6 min to produce a film of sufficient thickness for electrochemical experiments. We refer to this electrode as Cu-Feb. The differences with deposition time can change the structure of the electrode surface, which has been shown to affect product selectivity during CO<sub>2</sub> reduction, as demonstrated by the size-dependence of copper nanoparticles on hydrocarbon selectivity [29]. In addition, the difference in temperature may directly affect the product selectivity. For example, the Faradaic efficiency of CH<sub>4</sub> generation decreases and C<sub>2</sub>H<sub>4</sub> increases with increasing temperature [30].

FIG. 1 presents a series of IR spectra measured at different potentials for CO<sub>2</sub> reduction carried out in 0.1 mol/L NaHCO<sub>3</sub> at Cu-Jun. Several features are typical of CO<sub>2</sub> reduction on copper [28, 31–34]. Positive bands at 1650 and 3400 cm<sup>-1</sup> (not shown) can be attributed to the bending and OH stretching vibrations of water respectively [35]. The large negative band at 1550 cm<sup>-1</sup> is from the adsorbed electrolyte anion, and it consists of C–O stretching vibrations of adsorbed CO<sub>3</sub><sup>2-</sup> and HCO<sub>3</sub><sup>-</sup> [36]. The band is negative because the species adsorbed at the electrode surface during acquisition of the reference spectrum is desorbed as the potential is made more negative. HCO<sub>3</sub><sup>-</sup>/CO<sub>3</sub><sup>2-</sup> is not involved in the reaction directly, but its desorption makes it possible for CO<sub>2</sub> to access the electrode surface and be reduced [37]. The large band at 2080 cm<sup>-1</sup> corresponds to CO adsorbed in a linear configuration on the surface (CO<sub>L</sub>). It is first detected at -1.15 V, and it grows until the potential scan direction is reversed. The observation of CO on the electrode surface indicates that CO<sub>2</sub> has been reduced to CO.

In addition to these standard features, there are several smaller bands that are not often reported in literature. The small bands at 2940 and 2850 cm<sup>-1</sup> corre-

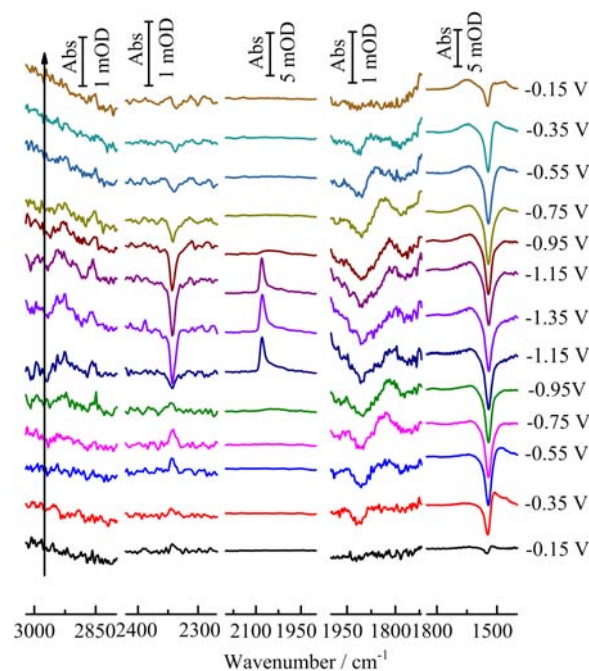


FIG. 1 IR spectra obtained during a cyclic voltammetric scan from -0.15 V to -1.4 V at the copper film electrode, Cu-Jun, deposited on a silicon prism in CO<sub>2</sub>-saturated 0.1 mol/L NaHCO<sub>3</sub>. The scan rate is 5 mV/s. The long black arrow indicates the direction of the potential scan. Scale bars above each wavenumber segment indicate the segments' respective absorbance scales. The reference potential is -0.15 V.

spond to the asymmetric and symmetric C–H stretches [36, 38]. In addition, there is a small band at 1850 cm<sup>-1</sup> that is likely to be the stretching vibration of C=O [39–41]. The presence of a negative band at slightly higher frequencies, which broadens as the potential is made more negative, suggests that some of this species has been already adsorbed to the electrode surface when the reference spectrum is obtained, and is either desorbed or shifted to lower frequencies as the potential is made more negative. Previous reports have attributed this band to bridge CO [37, 39, 41, 42] or to trace impurities in the electrolyte [27, 43]. Finally, the sharp band near 2340 cm<sup>-1</sup> corresponds to CO<sub>2</sub> near the electrode surface [34, 44]. When the potential becomes more negative, the band becomes more negative, indicating that CO<sub>2</sub> is reduced.

FIG. 2 shows the series of IR spectra obtained at the film, Cu-Feb. Other than the deposition time and the temperature, the experimental conditions are the same as those used to obtain the data shown in FIG. 1. The main difference between the results is that when using the Cu-Jun film, we can detect the CH band, but when using the Cu-Feb film, we cannot. As discussed earlier, the differences in temperature between the two months may affect the reaction, either through the change in surface structure caused by the difference in deposition

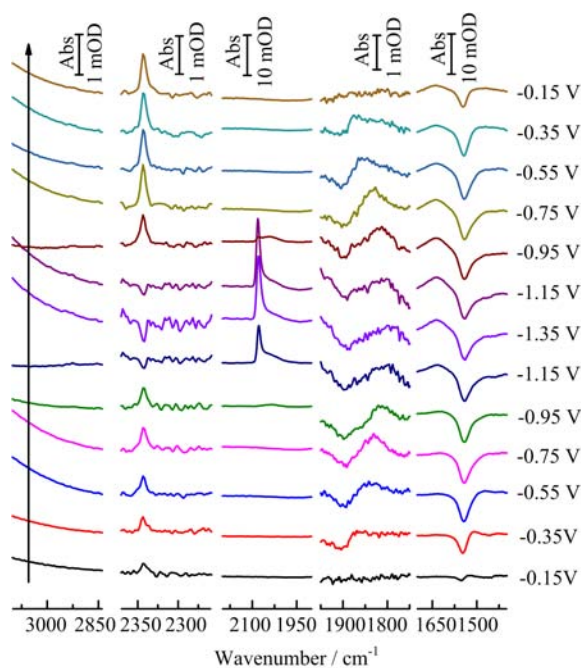


FIG. 2 IR spectra obtained during a cyclic voltammetric scan from  $-0.15$  V to  $-1.4$  V at the copper film electrode, Cu-Feb, deposited on a silicon prism in CO<sub>2</sub>-saturated 0.1 mol/L NaHCO<sub>3</sub>. The scan rate is 5 mV/s. The long black arrow indicates the direction of the potential. Scan scale bars above each wavenumber segment indicate the segments respective absorbance scale. The reference potential is  $-0.15$  V.

time, or by the change in the temperature at which the CO<sub>2</sub> reduction reaction occurs. In this solution, although the CO<sub>2</sub> band at 2340 cm<sup>-1</sup> decreases as the potential is made more negative, the band is positive at the start of the scan, indicating that the concentration was still increasing between the time the baseline was collected at and the time the first spectrum was collected at. This may result in a CO<sub>2</sub> concentration difference between the Cu-Feb measurement and the Cu-Jun measurement. The results are qualitatively the same, however. The primary effect of the different measurement time is that at higher temperature, more hydrocarbons are adsorbed on the electrode surface, as shown by the C-H bands that are only observable for the Cu-Jun sample. These bands are fairly small, suggesting that they do not occupy a large region of the surface. Therefore, we do not expect them to interfere significantly with the results of the CuPd experiments that are discussed in the remaining parts of this paper.

### B. Adsorbates generated during CO<sub>2</sub> reduction at CuPd film

To understand the differences in the behavior of CuPd and Cu for CO<sub>2</sub> reduction, we first carried out electrochemical ATR-FTIR measurements to examine

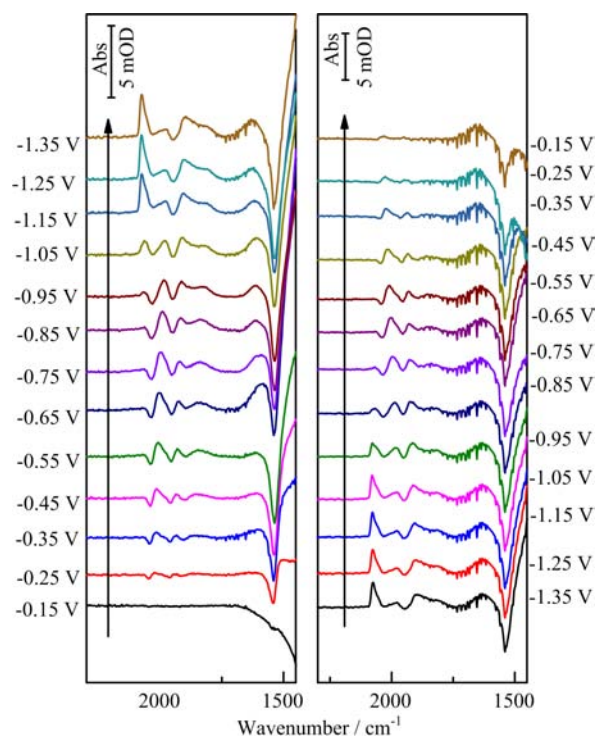


FIG. 3 IR spectra obtained during a cyclic voltammetric scan from  $-0.15$  V to  $-1.4$  V at a CuPd film electrode in CO<sub>2</sub>-saturated 0.1 mol/L NaHCO<sub>3</sub>. The scan rate is 5 mV/s. The long black arrows point the direction of the potential. Scan scale bars above each wavenumber segment indicate the segments respective absorbance scale. The reference potential is  $-0.15$  V.

adsorbates generated during CO<sub>2</sub> reduction at a CuPd film (FIG. 3). These experiments were all performed during winter and had the reaction characteristics of a low-temperature experiment, as discussed above. The band at 2080 cm<sup>-1</sup>, corresponding to CO adsorbed linearly on Cu, can be detected beginning at  $-0.95$  V. Another band can be seen at 2010 cm<sup>-1</sup>, beginning at  $-0.25$  V. Its frequency and its low onset potential are consistent with CO linearly adsorbed to Pd [45]. The band becomes stronger as the potential is made more negative, indicating increasing surface coverage of CO on Pd, and at very negative potentials, it partially overlaps with the bands attributable to linearly adsorbed CO, as well as a band at 1890 cm<sup>-1</sup>. When the potential is made positive again, the 2010 cm<sup>-1</sup> feature is still observed, indicating that CO<sub>L</sub> on Pd is not desorbed at these potentials. The 1890 cm<sup>-1</sup> band, discussed earlier, was attributed to a previously adsorbed C=O species on the electrode, but not to bridge CO (CO<sub>B</sub>), as there is no significant evidence that this species can be formed on copper. However, CO adsorbed to bridge and to threefold-hollow (CO<sub>T</sub>) sites on Pd has previously been reported [45]. As both of the C=O species observed on copper and the CO<sub>B</sub> and CO<sub>T</sub> species on Pd adsorb at similar potentials, we are unable to deter-

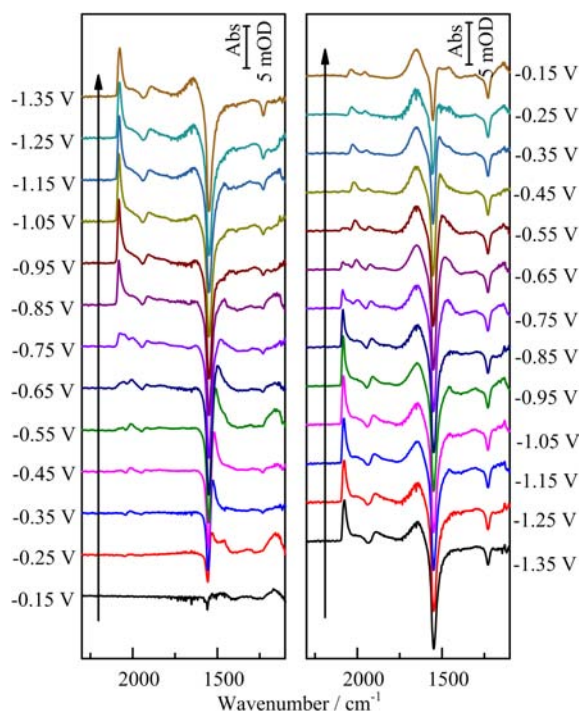


FIG. 4 IR spectra obtained during a cyclic voltammetric scan from  $-0.15$  V to  $-1.4$  V at a CuPd film electrode deposited on a silicon prism in CO-saturated  $0.1$  mol/L  $\text{NaHCO}_3$ . The scan rate is  $5$  mV/s. The long black arrow points the direction of the potential. Scan scale bars above each wavenumber segment indicate the segments respective absorbance scale. The reference potential is  $-0.15$  V.

mine which species is predominant. CH bands were not observed in any of the datasets involving CuPd. This may be due to the lower surface area of Cu, which reduces the size of the already-weak bands so that they are below the detection limit of our experimental setup.

Since our measurements of catalytic activity cannot be done in  $\text{CO}_2$ -saturated solution, due to problems with  $\text{CO}_2$  bubbles formed in the thin layer, we did the measurements in CO-saturated solution, in which CO is the reaction intermediate. In order to understand how this may affect the measured result, we also performed electrochemical ATR-FTIR measurements during CVs in CO-saturated  $0.1$  mol/L  $\text{NaHCO}_3$ . The IR spectra measured during a CV scanned from  $-0.15$  V to  $-1.4$  V are presented in FIG. 4. The bands previously observed in  $\text{CO}_2$ -saturated solutions are still observed in this solution. However, the onset potential for CO adsorption is around  $-0.5$  V. The onset potential is less negative for CO reduction because the energetically demanding conversion of  $\text{CO}_2$  to CO is not required in this case. Another difference is that the bands previously attributed to CO adsorbed to Pd, at  $1890$  and  $2010$   $\text{cm}^{-1}$ , are much weaker than those in the  $\text{CO}_2$ -saturated solution, although this may only indicate variation between measurements.

FIG. 5(a) shows the Faradaic currents measured at

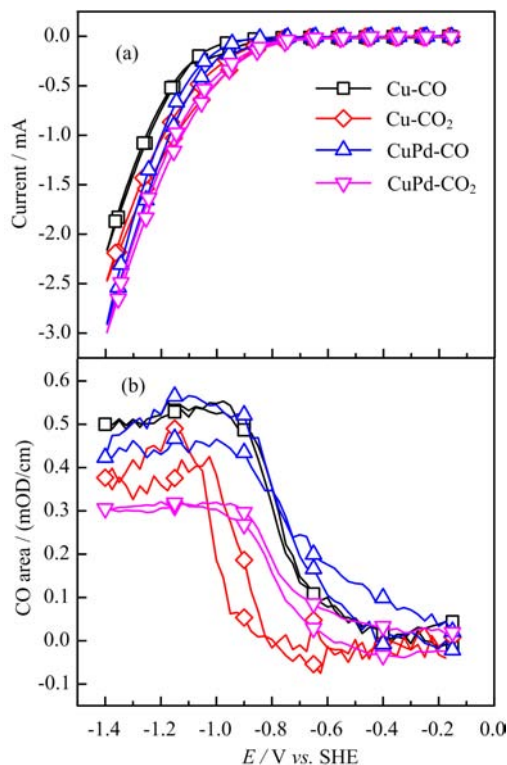


FIG. 5 (a) IR band integrals of the CO stretching vibration and (b) the faradaic current, measured during a CV scan Cu and CuPd film working electrodes in CO- and  $\text{CO}_2$ -saturated  $0.1$  mol/L  $\text{NaHCO}_3$  carried out at  $5$  mV/s.

Cu and CuPd electrodes as the electrode potential is swept negatively in CO- and  $\text{CO}_2$ -saturated solutions of  $0.1$  mol/L  $\text{NaHCO}_3$ . The Faradaic current is mostly attributed to hydrogen generation. In general, the current is higher in  $\text{CO}_2$ -saturated solution than that in CO-saturated solution, which is likely because the pH is  $6.8$  in  $\text{CO}_2$ -saturated solution and  $8.3$  in CO-saturated solution. The current is also generally higher at CuPd electrodes than that at Cu electrodes, which is likely because Pd is a better catalyst for  $\text{H}_2$  generation. FIG. 5(b) shows the integrals of the CO stretching bands of Cu- $\text{CO}_L$  measured during CVs carried out in CO- and  $\text{CO}_2$ -saturated solutions of  $\text{NaHCO}_3$  on Cu and CuPd electrodes with  $-0.15$  V as the anodic potential limit. The onset potential for the growth of the CO band measured on both catalysts in CO-saturated solution is almost the same ( $-0.5$  V). This means that the adsorption of CO on Cu and on the copper sites of CuPd is not likely controlled by the adsorption potential of CO on the respective metal, but by the desorption of the  $\text{HCO}_3^-/\text{CO}_3^{2-}$  anions that are initially adsorbed to the electrode surface [46]. However, the onset potentials for CO adsorption in the  $\text{CO}_2$ -saturated solution are different for each catalyst. On the pure Cu catalyst, the onset potential for the rise of the CO band is about  $-0.8$  V, whereas on CuPd, the onset potential is about  $-0.6$  V. This shows that the reduction of  $\text{CO}_2$  to CO on

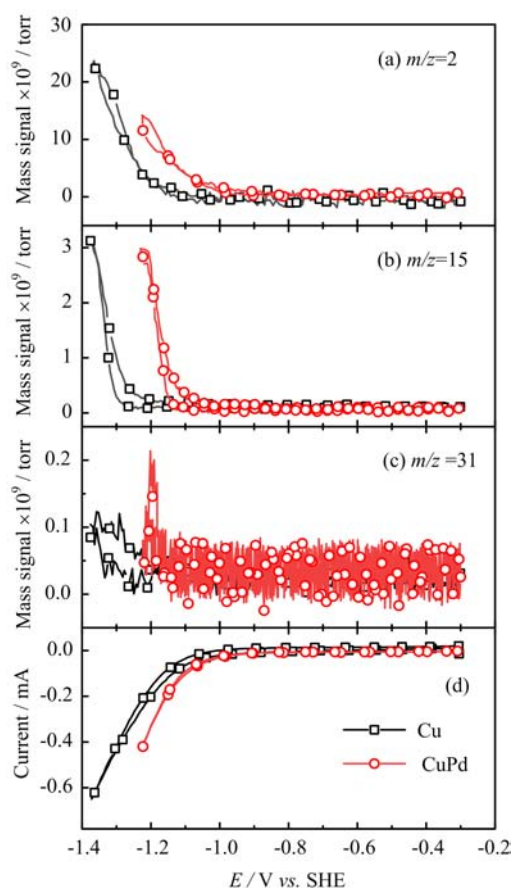


FIG. 6 Mass spectrometric signal of (a) hydrogen ( $m/z=2$ ), (b) methane ( $m/z=15$ ), (c) methanol ( $m/z=31$ ), and (d) the measured Faradaic current corresponding to CO reduction on polycrystalline Cu (black line) and CuPd (red line) during a CV scan in CO-saturated 0.1 mol/L NaHCO<sub>3</sub> carried out at 10 mV/s.

the Cu sites is significantly catalyzed by the presence of Pd.

### C. Volatile products generated during CO reduction on Cu and CuPd

In order to characterize the potential-dependence of product generation, we used DEMS to measure the volatile products generated in a CO-saturated solution for the Cu and CuPd electrodes. For both electrodes, the cathodic potential limit of the scan was determined by the potential at which the formation of hydrogen bubbles in the thin-layer cell caused the current to become unstable. The cyclic voltammograms carried out in 0.1 mol/L NaHCO<sub>3</sub> for both electrodes are presented in FIG. 6. The onset of reduction current (FIG. 6(d)) for CuPd occurs around  $-1.0$  V, whereas that for Cu begins around  $-1.1$  V. As discussed in FIG. 5(a), Faradaic current is mostly associated with hydrogen formation, and is therefore higher for the CuPd electrode, due to the strong adsorption of H atoms on Pd, and to a pos-

sible perturbation of the band energy of the Cu atoms as well. Theory shows that as the coordination number of Cu decreases, the d-band center shifts towards the Fermi level, resulting in stronger adsorption of H to the surface, and thus lowering  $\Delta G_H$ . Hence, in this case, the shift of the d-band center can be used to explain the enhancement of HER on CuPd [23].

The onset potentials for methane ( $m/z=15$ , FIG. 6(b)) and methanol ( $m/z=31$ , FIG. 6(c)) formation are about 200 mV more positive on the copper foil than those on the CuPd electrode. This positive shift in the onset potential for product generation is attributed to the greater ability of Pd to bind hydrogen which is a necessary component for converting adsorbed CO to hydrocarbons [24]. This description explains why even though CuPd and Cu appear to adsorb similar amounts of CO at the reactive Cu sites, CuPd is able to generate hydrocarbon products, such as CH<sub>4</sub> and CH<sub>3</sub>OH, more efficiently than Cu alone.

## IV. CONCLUSION

In this work, we used DEMS and ATR-FTIR spectroscopy to examine the differences in the adsorbates and volatile products generated during CO and CO<sub>2</sub> reduction on Cu and CuPd electrodes. Our ATR-FTIR spectroscopy results show that the conversion of CO<sub>2</sub> to CO adsorbed on reactive Cu sites is more favorable on CuPd than on pure Cu. This is attributed to the interaction of Cu with nearby Pd atoms, which shifts the d-band center for the Cu atoms in the bimetallic catalyst. Interestingly, in CO-saturated solution, both metals show the same onset potential for the adsorption of CO. Despite the similar surface coverages of CO on both catalysts, our DEMS results show that the onset potential of CO reduction is 200 mV more positive on CuPd than that on a Cu foil. We attribute this difference to the increased adsorption of hydrogen on Pd, which provides a source for the H atoms needed to convert CO to hydrocarbons. For CO<sub>2</sub> reduction, the bimetallic catalyst, CuPd is more effective than Cu because it has a lower activation barrier for the reduction of CO<sub>2</sub> to adsorbed CO and catalyzes more rapid conversion of CO to hydrocarbons.

## V. ACKNOWLEDGMENTS

This work was supported by the National Natural Science Foundation of China (No.91545124 and No.21750110437). Matthew McCullough Sartin is supported by the Chinese Academy of Sciences President's International Fellowship Initiative (No.2017PM0049).

- [1] Y. J. Zhang, V. Sethuraman, R. Michalsky, and A. A. Peterson, ACS Catal. **4**, 3742 (2014).

- [2] R. Kortlever, J. Shen, K. J. P. Schouten, F. Calle-Vallejo, and M. T. Koper, *J. Phys. Chem. Lett.* **6**, 4073 (2015).
- [3] I. V. Chernyshova, P. Somasundaran, and S. Ponnurangam, *Proc. Natl. Acad. Sci. USA* **115**, E9261 (2018).
- [4] H. Mistry, A. S. Varela, S. Kühn, P. Strasser, and B. R. Cuenya, *Nat. Rev. Mater.* **1**, 1 (2016).
- [5] D. Gao, F. Cai, G. Wang, and X. Bao, *Curr. Opin. Green. Sustain. Chem.* **3**, 39 (2017).
- [6] J. H. Wu, Y. Huang, W. Ye, and Y. G. Li, *Adv. Sci.* **4** (11) (2017).
- [7] K. Lee, H. Kosaka, S. Sato, T. Yokoi, B. Choi, and D. Kim, *J. Ind. Eng. Chem.* **72**, 73 (2019).
- [8] H. Wang, P. Gao, T. Zhao, W. Wei, and Y. Sun, *Sci. China. Chem.* **58**, 79 (2014).
- [9] Z. Sun, M. M. Sartin, W. Chen, F. He, J. Cai, and Y. X. Chen, *J. Phys. Chem. C* **123**, 21467 (2019).
- [10] Y. J. Zhang, V. Sethuraman, R. Michalsky, and A. A. Peterson, *ACS Catal.* **4**, 3742 (2014).
- [11] J. Yang, J. Wei, W. Chen, and Y. X. Chen, *Chin. J. Chem. Phys.* **31**, 626 (2018).
- [12] Y. Hori, A. Murata, and R. Takahashi, *J. Chem. Soc. Farad. Trans.* **85**, 2309 (1989).
- [13] Y. Katayama, F. Nattino, L. Giordano, J. Hwang, R. R. Rao, O. Andreussi, N. Marzari, and Y. Shao-Horn, *J. Phys. Chem. C* **123**, 5951 (2018).
- [14] F. Y. Zhang, T. Sheng, N. Tian, L. Liu, and S. G. Sun, *Chem. Commun.* **53**, 8085 (2017).
- [15] C. W. Li and M. W. Kanan, *J. Am. Chem. Soc.* **134**, 7231 (2012).
- [16] A. Banerjee, G. R. Dick, T. Yoshino, and M. W. Kanan, *Nature* **531** (2016).
- [17] Y. Huang, A. D. Handoko, P. Hirunsit, and B. S. Yeo, *ACS Catal.* **7**, 1749 (2017).
- [18] D. Gao, I. Zegkinoglou, N. J. Divins, F. Scholten, I. Sinev, P. Grosse, and B. R. Cuenya, *ACS Nano* **11**, 4825 (2017).
- [19] T. Takashima, T. Suzuki, and H. Irie, *Electrochim. Acta* **229**, 415 (2017).
- [20] M. Li, J. Wang, P. Li, K. Chang, N. Umezawa, and J. Ye, *J. Mater. Chem. A* **4**, 4776 (2016).
- [21] J. Aldana-González, J. Olvera-García, M. G. M. Oca, M. Romero-Romo, M. T. Ramírez-Silva, and M. Palomar-Pardavé, *Electrochem. Commun.* **56**, 70 (2015).
- [22] R. Reske, M. Duca, M. Oezaslan, K. J. P. Schouten, M. T. M. Koper, and P. Strasser, *J. Phys. Chem. C* **4**, 2410 (2013).
- [23] R. Jana, A. Bhim, P. Bothra, S. K. Pati, and S. C. Peter, *Chemsuschem* **9**, 2922 (2016).
- [24] Y. Hori, A. Murata, and Y. Yoshinami, *J. Chem. Soc. Farad. Trans.* **87**, 125 (1991).
- [25] M. Dunwell, Q. Lu, J. M. Heyes, J. Rosen, J. G. Chen, Y. Yan, F. Jiao, and B. Xu, *J. Am. Chem. Soc.* **139**, 3774 (2017).
- [26] A. Wuttig, M. Yaguchi, K. Motobayashi, M. Osawa, and Y. Surendranath, *Proc. Natl. Acad. Sci. USA* **113**, E4585 (2016).
- [27] M. M. Sartin, Z. Yu, W. Chen, F. He, Z. Sun, Y. X. Chen, and W. Huang, *J. Phys. Chem. C* **122**, 26489 (2018).
- [28] H. F. Wang, Y. G. Yan, S. J. Huo, W. B. Cai, Q. J. Xub, and M. Osawa, *Electrochim. Acta* **52**, 5950 (2007).
- [29] R. Reske, H. Mistry, F. Behafarid, B. R. Cuenya, and P. Strasser, *J. Am. Chem. Soc.* **136**, 6978 (2014).
- [30] Y. Hori, K. Kikuchi, A. Murata, and S. Suzuki, *Chem. Lett.* **15**, 897 (1986).
- [31] Y. Hori, H. Wakebe, T. Tsukamoto, and O. Koga, *Surf. Sci.* **335**, 258 (1995).
- [32] Y. Hori, A. Murata, T. Tsukamoto, H. Wakebe, O. Koga, and H. Yamazaki, *Electrochim. Acta* **39**, 2495 (1994).
- [33] Y. Hori, O. Koga, Y. Watanabe, and T. Matsuo, *Electrochim. Acta* **44**, 1389 (1998).
- [34] S. Zhu, B. Jiang, W. B. Cai, and M. Shao, *J. Am. Chem. Soc.* **139**, 15664 (2017).
- [35] M. Baldassarre and A. Barth, *Analyst* **139**, 2167 (2014).
- [36] T. Iwasita and E. Pastor, *Electrochim. Acta* **39**, 531 (1994).
- [37] A. Wuttig, C. Liu, Q. Peng, M. Yaguchi, C. H. Hendon, K. Motobayashi, S. Ye, M. Osawa, and Y. Surendranath, *ACS Cent. Sci.* **2**, 522 (2016).
- [38] B. D. Smith, D. E. Irish, and J. Augustynski, *J. Electrochem. Soc.* **144**, 4288 (1997).
- [39] J. Salimon, R. M. Hernández-Romero, and M. Kalaji, *J. Electroanal. Chem.* **538-539**, 99 (2002).
- [40] S. K. Shaw, A. Berná, J. M. Feliu, R. J. Nichols, T. Jacob, and D. J. Schiffrin, *Phys. Chem. Chem. Phys.* **13**, 5242 (2011).
- [41] C. M. Gunathunge, V. J. Ovalle, Y. Li, M. J. Janik, and M. M. Waegle, *ACS Catal.* **8**, 7507 (2018).
- [42] S. K. Shaw, A. Berná, J. M. Feliu, R. J. Nichols, T. Jacob, and D. J. Schiffrin, *Phys. Chem. Chem. Phys.* **13**, 5242 (2011).
- [43] M. Dunwell, X. Yang, Y. Yan, and B. Xu, *J. Phys. Chem. C* **122**, 24658 (2018).
- [44] W. W. Rudolph, D. Fischer, and G. Irmer, *J. Appl. Spectrosc.* **60**, 130 (2006).
- [45] H. Miyake, E. Hosono, M. Osawa, and T. Okada, *Chem. Phys. Lett.* **428**, 451 (2006).
- [46] M. M. Sartin, W. Chen, F. He, and Y. X. Chen, *J. Electrochem.* 10.13208/j.electrochem.181242.